Searching for the rate determining step of the H2S reaction on Fe (110) surface

Salawu Omotayo Akande, El Tayeb Bentria, Othmane Bouhali, Fedwa El-Mellouhi

Applied Surface Science 532 (2020) 147470

Contents lists available at ScienceDirect

Applied Surface Science

journal homepage: www.elsevier.com/locate/apsusc

Searching for the rate determining step of the H_2S reaction on Fe (110) surface

Salawu Omotayo Akande[a], El Tayeb Bentria[b], Othmane Bouhali[a], Fedwa El-Mellouhi[b,*]

[a] Texas A & M University at Qatar, PO Box 23874, Doha, Qatar
[b] Qatar Environment and Energy Research Institute, Hamad Bin Khalifa University, PO Box 34110, Doha, Qatar

ARTICLE INFO

Keywords:
Adsorption
Metal dusting
Corrosion
Hydrogen sulphide
Catalyst
Density functional theory

Abstract: The adsorption and dissociation of H_2S on Fe surface play a key role in carburization condition and a detailed understanding of the kinetics and rate-determining step of this process from an atomistic modeling perspective will help in understanding better ways of mitigating metal dusting. Hence, we employed first-principles density functional theory with a correction for the long-range interactions to investigate H_2 reaction on Fe (110) surface. We probed the role of orientation of H_2S on adsorption energetics, elementary pathways and dissociation barriers on Fe(110) surface. We report the geometries and energetics of an exhaustive set of molecular and fragmented states induced by the different orientations of H_2S on Fe (110) surface. Our investigation further revealed that H_2S can be either adsorbed as a molecule, as HS + H, or even as H/S/H atoms depending on the orientation of the molecule and the site of adsorption. In addition, we calculated the rate of adsorption and dissociation to resolve the competition between adsorption sites, and found that the complete decomposition can commence from either the long bridge or short bridge sites.

1. Introduction

Metal dusting defines the corrosive disintegration of metals and alloys into fine particles and graphite in a carbon saturated environment at high temperature. This phenomenon has been reported for metals having synthetic gases flowing through them. It is prevalent in pressure vessels and heat exchangers used in the oil and gas industry [1]. When metals/alloys dissolve carbon and do not form stable carbides in a carbon saturated environment, they lead to the formation of graphite and the eventual destruction of the materials [2,3]. This process begins with the adsorption of carbon at the surface then diffusion of the adsorbed carbon into the sub-surface thereby forming carbides. This is succeeded by the appearance of a layer of coke at the surface, which consequently impairs heat transfer, reduces catalytic lifetime and eventually weakens the integrity of the structure. For instance, metal dusting was reported for CR-B configuration at waste heat boilers in a gas to liquid (GTL) plant where the deposition of catalyzed carbon lead to the initiation of degradation of metals and alloys, eventually resulting in formation of a dust of fine particles [4]. Experiments have shown that for Fe, the transfer of carbon into solid solution leads to the saturation of the Fe phase thereby allowing the growth of cementite at defected surfaces and grain boundaries [3]. Note that the cementite formed impede the further diffusion of carbon, however, when the activity of C is increased, the cementite becomes unstable and begin to decompose leading to the formation of fine Fe dust.

The serious economic and environmental implication of the metal dusting process especially in the oil and gas sector have attracted interest in the design of systems that are efficient at inhibiting this type of corrosion [2,5,6]. Some of the mechanisms put forward to control the dusting include alloying, aiming at the formation of high performance oxide scale, decrease carbon precipitation, and surface engineering. Another route examines the role of adding Sulfur(S)-based gases (H_2S, CS_2) to the environment where this reaction takes place [7,8]. The presence of H_2S in a carburizing environment can trigger the adsorption of S on the Fe surface which in turn leads to the retardation of the transfer of C since the adsorbed S blocks the reaction sites involved in carburization. This effect is of great importance for instance in reactors in the steam-cracking of hydrocarbons [9]. Indeed, it has also been demonstrated that H_2S dosing (< 1 ppm) retards the carburization of cracking tubes [7]. Also, S is known to adsorb on cementite surface thereby suppressing graphite nucleation and consequently stopping graphite nucleation overtime [10]. In order to effectively utilize this approach, it is important to understand the retardation procedure induced by H_2S dosing.

Thermogravimetric analysis showed that the level of retardation of metal dusting is heavily dependent on temperature, carbon activity and

* Corresponding author.
E-mail address: felmellouhi@hbku.edu.qa (F. El-Mellouhi).

https://doi.org/10.1016/j.apsusc.2020.147470
Received 7 May 2020; Received in revised form 16 July 2020; Accepted 4 August 2020
Available online 09 August 2020

H_2S content [11]. Specifically, the amount of H_2S required to suppress metal dusting is proportional to the activity of carbon [12,13]. Although H_2S in large dose is known to aggressively attack metals, [14] the kinetics of the reaction showed that the rate of surface reaction that lead to carburization is proportional to the surface area occupied by S, one S atom appears to be sufficient to block one reaction site for the dissociation of CO. The ability of S to block the reaction sites not withstanding, the inherent presence of defects in the S monolayer allows it to retard the carburization thus, while S can slow down carburization, it cannot fully stop the process [13]. Previous experimental studies on the reaction of H_2S with poly-crystalline Fe reported molecular adsorption of H_2S at 100 K and found dissociated state above 190 K [15–17]. Same research also showed that above 423 K iron sulfide(FeS) is formed upon increase in H_2S dosing. Another experiment using low energy electron diffraction (LEED) studied the deposition of S on Fe(110) and reported S forming a p(2X2) pattern [18]. Interestingly, none of these experiments reported molecular adsorption of H_2S at room temperature or above and this indicates the fast dissociation of H_2S on Fe surface. Density functional theory investigation presented H_2S to be weakly adsorbed on Fe(100) surface [14]. Hence, there is a need for the understanding of the H_2S dissociation process at atomic scale level and unraveling the key processes governing its reaction with the surface. Understanding the interaction between the gases involved and the metal surface is key to characterizing this degradation mechanism and ultimately, the design of dusting-resistant materials. The interaction of H_2S with Fe(110) surface might occur following a series of reactions leading to its complete decomposition [19,20]:

$$Fe(110) + H_2S \rightarrow Fe(110) + H_2S_{adsorbed} \quad (1)$$

$$Fe(110) + H_2S_{adsorbed} \rightarrow Fe(110) + HS^{-}_{adsorbed} + H^{+}_{adsorbed} \quad (2)$$

$$Fe(110) + HS_{adsorbed} + H_{adsorbed} \rightarrow Fe(110) + S^{-}_{adsorbed} + 2H^{+}_{adsorbed} \quad (3)$$

The process occurs at extreme conditions, hence investigating the rate determining step of this process is crucial, in other words, there is need for microscopic understanding of the kinetics of the overall reaction. Furthermore, increasing the H_2S content in carburizing atmosphere lead to a decrease in CO reaction speed hence underlining the role of coverage on kinetics of this reaction. The effect of the H_2S coverage on the reaction energetics remain elusive. Theoretical and computational approaches have been successfully applied to characterize key catalytic processes [21–24]. Specifically, density functional theory (DFT), molecular dynamics (MD) and other computational methods have been used to study adsorption and dissociation of H_2S on Fe surfaces and other metallic surfaces [25–29] Carter and coworkers [14,30] studied the adsorption and dissociation of H_2S on Fe surfaces. They reported that while the first dehydrogenation of H_2S (reaction 2) require overcoming barriers of 0.25 eV on Fe (100) surface [30], the process is almost barrierless on the Fe (110) surface [14]. Recently, Fang and coworkers [31] also examined the role of vacancy on the adsorption and dissociation of H_2S on Fe (100) surface. They reported a dissociation barrier of 0.35 eV and 0.28 eV for the first and second dehydrogenation of H_2S (reactions 2 and 3 respectively). In addition, they found H_2S to be stable when adsorbed at the bridge aligned vertical to the Fe(100) surface which contrary to the conclusion of Carter and coworkers the H_2S was found to be horizontally aligned as explained above. While all of these previous works have made effort to describe the adsorption process and reported barriers for dissociation, there are variations in the calculated results and conclusions reached. Notably, one would intuitively expect that Fe (100) a more open surface compared to Fe (110) surface would present a lower H_2S dissociation barrier than the later. However, previous reports suggest the opposite [14,30]. In view of the inconsistencies, it has become necessary to examine the origin of the minima used as the initial and final configurations to calculate the barriers as this hugely determines the barrier calculations. We focus here on two key aspects overlooked in previous studies. First, different authors [14,30,25] have different starting positions and arrived at different conclusions, hence we perform a systematic analysis of the effect of H_2S orientation on Fe surface impacting the adsorption and dissociation energetics. Subsequently, we investigate the rate determining step of the reaction of Fe(110) surface.

2. Computational details

We performed density functional theory calculations using the Vienna Ab-initio Simulation Package (VASP) [32] and the Perdew-Burke-Ernzerhof (PBE) exchange–correlation functional [33]. The adsorption of polar molecules on a metallic surface requires the inclusion of van der Waals dispersion (vdW) interaction since it plays an important role in the molecule/metal bonding [34,35]. We take this into consideration in this work using the Grimme DFT-D3 method [36]. An energy cut-off of 400 eV was used to expand the plane-wave basis set. Spin polarization was taken into account to describe correctly magnetic properties of the Fe systems and self consistency achieved with a total energy convergence of 1×10^{-5} eV. Bulk Fe was modeled using a body centered-cubic structure with space group $Im\bar{3}m$ with lattice constant 2.83 Å. The Fe(110) surface was cleaved starting from the optimized bulk structure and a vacuum of 11 Å along the *c*-axis was added which was found to be sufficient to avoid interaction between slabs due to periodic boundary conditions. In addition, convergence test carried showed that five layers are sufficient to reliably model H_2S adsorption on Fe(110). Hence all the adsorption investigation in this work are based on five Fe layers thick slab with the top two layers allowed to relax while the bottom three fixed at the bulk-truncated condition. The H_2S and top two layers of the Fe(110) surface were fully relaxed until the residual forces on each atom reached 0.01 eV/Å. The Brillouin zone was sampled by a $9 \times 9 \times 1$ Monkhorst–Pack k-point mesh. We modeled the H_2S free molecule using a $15 \times 15 \times 15$ cell thereby obtaining an optimized H-S bond length of 1.35 Å and H-S-H angle of 92°. The obtained bond length and angles are in agreement with previous works [14,24].

Furthermore, in order to investigate the role of H_2S concentration on the adsorption kinetics, we consider slabs with one H_2S molecule adsorbed on a 2×2 (40 atoms) corresponding to a coverage of 0.25ML and 4×4 (160 atoms, 0.0625ML) representing a regime of high and low coverage respectively. To obtain optimized adsorption configurations with minimum energy on the Fe(110) surface, our model takes into account the different possible orientation of the H_2S molecule as well as all possible high symmetric surface positions of adsorption. We used Pymatgen [37] adsorption locator to determine all possible adsorption sites. The Pymatgen module provides classes used to enumerate different possible adsorption sites on a slab. We manipulated the orientation of H_2S molecule on the different sites resulting from this module. First, the algorithm was used to select high symmetric surface sites, then a 2D Voronoi tessellation of the coordinates of this surface sites projected on the plane perpendicular to the miller index are calculated. For the Fe(110) surface, the on-top (OT), short bridge (SB), long bridge (LB) and three fold hollow (TF) are obtained confirming adsorption sites previously used for adsorption on this surface [24]. The sites obtained using Pymatgen are as shown in Fig. 1(a). The different H_2S molecule rotations (R) and flips (F) considered are shown in Fig. 1(b). For rotation, H_2S is made to rotate from vertical position on the Fe surface at interval of 45 degrees and the flip configurations also follow similar pattern. We found seven(7) unique H_2S rotation/flip configurations, summing up to a total of 28 configurations for the four adsorption sites considered. The nomenclature used here to describe adsorption is as follows: The rotation/flip operation on the molecule can either be a "R" (rotation) or a "F" (flip) using angles 00,45° or 90° situated at either the Top (OT), short bridge (SB), long bridge (LB) or threefold (TF). Hence, in the rest of this paper, configurations will be referred to in terms of (R/F)(00/45/90)@(OT/SB/LB/TF). Note that there are two variants of the F at 45° and are here referred to as F45 and

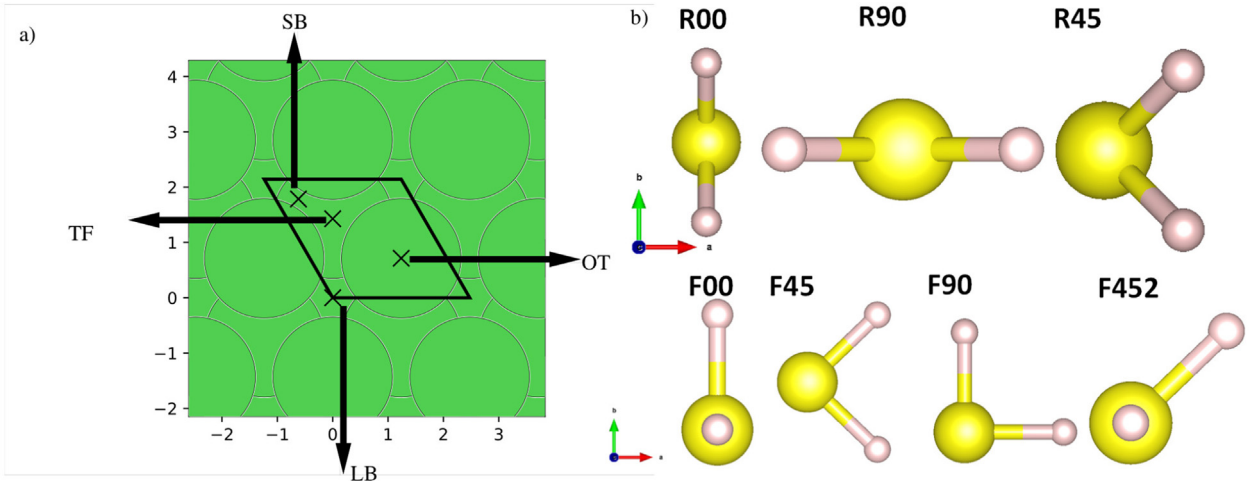

Fig. 1. (a) High symmetry positions of adsorption identified by Pymatgen for Fe(110) surface (b) Top shows the 3 rotation (R) configuration of the H_2S molecule, bottom shows the flip (F) configurations and their corresponding angles in degrees. Refer to the text for the abbreviations.

$F45_2$.

The Climbing-image nudged elastic band (CI-NEB) method [38,39] was subsequently employed to compute the minimum energy paths (MEP) and transition states associated with the rotation, translation and dissociation mechanism of H_2S molecule. The rate of adsorption/dissociation of H_2S on Fe(110) surface can be expressed in an Arrhenius form as

$$R = Ae^{-E_a/k_BT} \tag{4}$$

where E_a is the activation energy of adsorption/dissociation, k_B is the Boltzman constant and T is temperature in Kelvin. A is a pre-exponential factor that includes the partition functions and frequencies. The pre-exponential factor can be calculated for the reaction and is defined as

$$A = \frac{k_bT}{h}\frac{Q^{TS}}{Q} \tag{5}$$

Here, k_b and h are the Boltzmann and Planck's constants, respectively, T the temperature (in K), and Ea the electronic activation energy. Q^{TS} and Q refer to the partition functions of the transition state and the ground state, respectively. This formalism has been used to estimate rates of reactions in previous works [40,41].

3. Results and discussion

We first validate our approach against known properties of bulk α-Fe BCC. Our calculation of the α-Fe bulk structure yields a lattice constant of 2.84 Å differing by only 2% from experimental measurement and magnetic moment of 2.214 μ_B, in good agreement with previous work [14]. Analysis of the surface reconstruction and its effects have been presented in our previous work [24]. We showed that among the possible facets of the Fe surface, the Fe(110) surface possess the least amount of reconstruction with only 0.04–0.10% change in the inter-layer spacing from the surface with respect to the bulk inter-layer spacing.

3.1. Molecular H_2S adsorption

Molecular adsorption of H_2S on Fe(110) surface might occur starting from various configurations. However, certain molecular orientations are more favored than others based on how they interact with the Fe surface. To estimate the adsorbate–surface interaction, we compute the adsorption energy according to:

$$E_{ads} = E_{H_2S/slab} - E_{slab} - E_{H_2S}, \tag{6}$$

where $E_{H_2S/slab}$, E_{slab} and E_{H_2S} are the total energies of the adsorbed species, clean Fe(110) surface and the molecular H_2S respectively.

From the 28 configurations initially considered for H_2S adsorption on Fe(110), only 14 initial configurations resulted in H_2S molecular adsorption after full geometric optimization. Matching the pattern obtained for the 14 initial configurations after relaxation with the nomenclature described earlier, we end up with five orientations shown in Fig. 2. The TF site was also found to be generally unstable for molecular H_2S adsorption as all starting configurations on this site often relax to the LB site. Worth mentioning that the difference in adsorption for 2 configurations with same molecular orientation stem from the difference in the distance between the molecule and surface. We report here the configurations with the lowest energy for each orientation. The structures are shown in Fig. 2 and their adsorption energies and geometric properties presented in Table 1. The adsorption of H_2S molecule on Fe(110) surface is evidently exothermic with our calculation revealing a relatively weak adsorption. Typical orientations of H_2S on the OT site are as shown in Figs. 2(a) and (b), both structures having different orientation of the H_2S molecule. Note that our calculation obtained results that are in agreement with previous work for the same orientation of the H_2S molecule. Fig. 2(c) shows a structure equivalent to the minima found in previous work where we found same adsorption energy as the one found in previous work [30]. It is 0.1 eV less stable compared to R00@SB and R45@LB, the most stable configurations found from our calculation (Figs. 3(d) and (e) respectively). The R45@LB configuration has the H_2S interacting with two adjacent Fe atoms resulting from rotation of the H_2S thereby leading to elongation of the H-S bond by 0.05 Å compared to the free standing H_2S molecule and consequently having the H atoms attracted to the Fe surface. Similarly, in the case of the R00@SB, H_2S interact with 2 Fe atoms on the surface and upon relaxation, the H_2S reoriented 45 degrees across the surface, although still situated at the starting SB position. Generally, The LB site is the most stable site for molecular H_2S adsorption. Our calculated adsorption energies for the 5 unique configurations vary from −0.60 to −0.296 eV and are lower than the adsorption energy of H_2S on Fe(100) (−0.46 to −0.13 eV)[14], suggesting a stronger interaction for H_2S/Fe (110) than H_2S/Fe(100). The highest adsorption energies are found for molecules located at the OT sites indicating that these sites are the least favorable for H_2S molecular adsorption. The H_2S/Fe(110) is similar to the H_2S/ Rh(110)[42] interaction by binding favorable to the LB site, although the latter adsorption is stronger. The effect of coverage on the trends discussed here are addressed in the supplementary material attached to this paper.

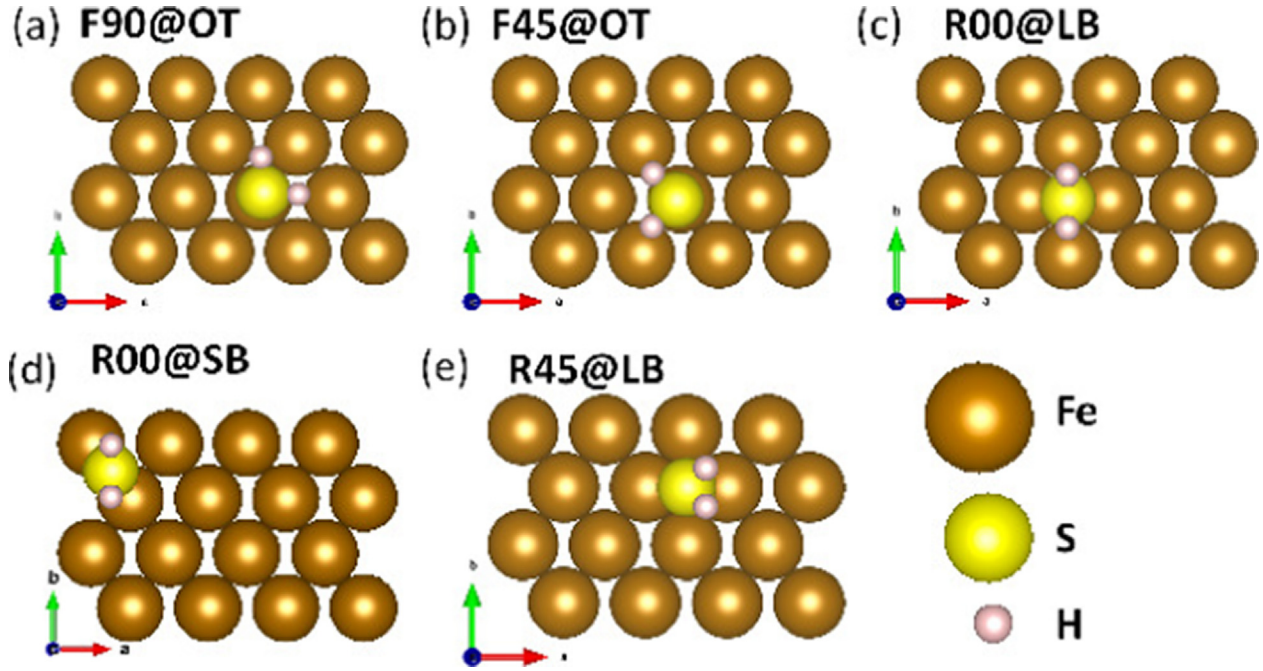

Fig. 2. Top view representation of the five distinct states of H_2S molecular adsorption on Fe(110) surface. Fe is shown in gold spheres, sulfur in yellow and hydrogen in pink. (For interpretation of the references to colour in this figure legend, the reader is referred to the web version of this article.)

Table 1
Adsorption energies and geometrical parameters such as bond length and angles for molecular H_2S adsorption on Fe(110) at a coverage of 0.25ML.

Configuration	E_{ads} (eV)	H-S (Å)	Fe-S (Å)	H-S-H (°)
F90@OT	-0.30	1.36	2.28	91.52
F45@OT	-0.45	1.36	2.28	90.66
R00@LB	-0.49	1.36	2.23	90.42
R00@SB	−0.59	1.37	2.24	92.70
R45@LB	−0.60	1.38	2.24	90.45

3.2. Fragmented adsorption (H + HS and H/S/H)

For certain orientations of H_2S molecule on Fe (110) surface, the adsorption occur in fragmented form whereby one or both of the H-S bond break spontaneously. Only few initial structures lead to the case of adsorption where just one of the H-S is bond is broken. In fact, this mode of adsorption is realized for the bridge sites SB and LB only. Hence, the structures relaxing to this configuration are fewer than those obtained in the previous configuration, totaling three configurations starting as $F45_2$@SB, F00@SB and F00@LB lead to this form of

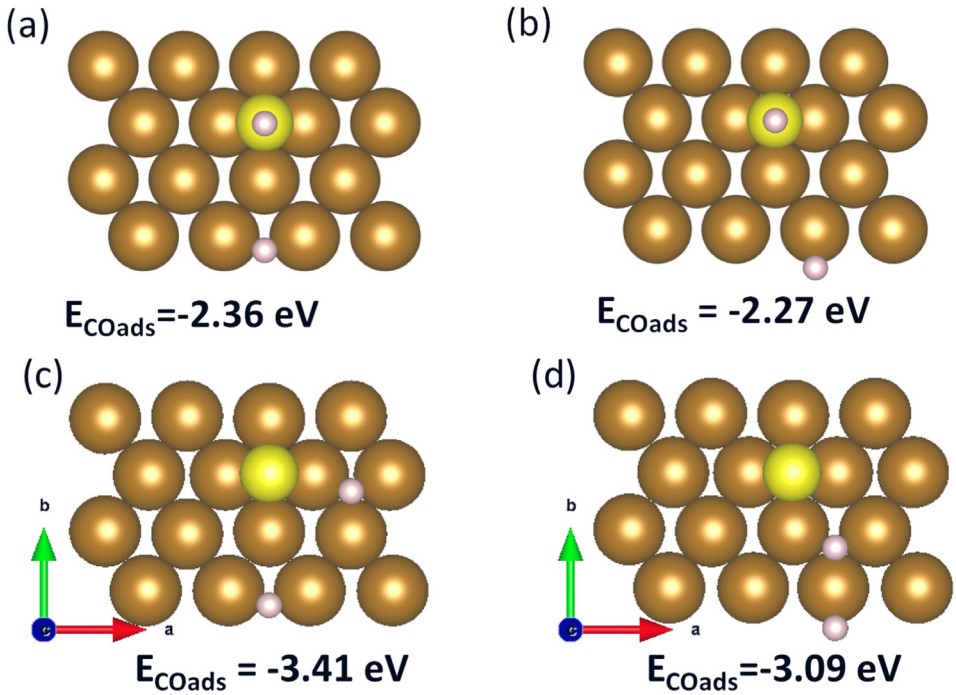

Fig. 3. Top view representation of the distinct states of co-adsorption. Color coding is as described in Fig. 2. (For interpretation of the references to colour in this figure legend, the reader is referred to the web version of this article.)

fragmented adsorption. The final structures and their corresponding adsorption energies are as shown in Fig. 3(a and b). For the F00@SB, relaxation process lead to translation of the molecule to LB site and fragmentation of the H atom closest to the Fe surface with both the atomic hydrogen and HS moiety prefer the LB. Similarly, for F452@LB the relaxation process leads to a simple fragmentation of the H atom closest to the Fe surface with HS moiety relaxing to the LB position and the atomic H pushed to the TF location thereby decreasing its energy by 0.09 eV. The behavior of the adsorbed moieties agree well with those reported in previous theoretical work where the preference of the LB site for HS adsorption have been reported [14].

The complete dissociation of the H_2S into H, S, H atoms is obtained for 11 out of the 28 initial configurations considered, Fig. 3(c and d) shows two representative structures. Analysis of the adsorption energy shows degeneracy in most of the 11 initial configurations that relaxed in this mode of adsorption. In the resulting structures, the three atoms most often occupy similar positions and only differ by their distance to the surface. The Most stable configuration is found for a case where hydrogen atoms occupies TF and S is localized at the LB position. Therefore, the H atom prefer the TF site, while the S atom prefers the LB site in agreement with previous work on adsorption of H_2S on Fe(110) surface [14].

From our analysis of the different adsorption scenarios for the reaction of H_2S on Fe(110), it is evident that while certain configurations are more favored, the degeneracy found for the most stable configurations make it difficult to ascribe preferential adsorption site to a particular site. Our calculation predicted a 0.01 eV difference in adsorption between the R45@LB and R00@SB. We doubt that this very small difference can have significant implication on conclusions reached with respect to the overall reaction on the Fe(110) surface. One scenario where the effect of this small energy difference is quantified is by calculating the chance of sticking of the H_2S molecule on these configurations. To this end we calculate the rate of adsorption of the 5 sites shown in Fig. 2 and obtain the competition between these sites assuming that the adsorption to each of these sites occur simultaneously. The rate of adsorption is shown in Table 2 and the percentage of molecule sticking on the surface for each site is shown in Fig. 4. Analysis of this competition shows that at 300 K, 59% of the molecule sticks for R45@LB while 40% stick on R00@SB. At 700 K, while this percentage is reduced significantly for R45@LB to 48%, R00@SB still maintains 40% and R00@LB has 8% sticking chance, which is further boosted to 12% upon increasing temperature to 1100 K. Overall, in the temperature range considered (300, 700 and 1100 K) adsorption at R45@LB dominates. However, note that at very high temperature (1100 K) H_2S has equal chance of sticking to both the R45@LB and R00@SB sites. This implies that the dissociation of H_2S can begin from either of these two sites, hence any complete description of the dissociation of H_2S on Fe(110) have to take into account these two sites.

For each of the mode of adsorption, further calculations are carried out for only the most energetically favorable structures. We only consider multiple structures in cases where we find competition in energetics.

Table 2
Adsorption rate constant (s^{-1}) for the adsorption H_2S at different temperature in K.

Configuration	300 K	700 K	1100 K
F90@OT	1.6×10^5	1.7×10^2	2.6×10^1
F45@OT	6.6×10^7	2.2×10^3	1.4×10^2
R00@LB	3.2×10^8	4.4×10^3	2.1×10^2
R00@SB	1.7×10^{10}	2.4×10^4	6.2×10^2
R45@LB	2.6×10^{10}	2.9×10^4	6.9×10^2

3.3. Minimum energy path for complete H_2S dissociation

In methods such as the nudged elastic band model, mapping the minimum energy path (MEP) requires knowing the initial and final states a priori. Hence it is important to meticulously choose the initial and final configurations. Given the large number of starting points arising from the adsorption site as well as molecular orientation with respect to the surface, a large number of possibilities are available for exploration. However, our extensive exploration of the minima enables us to map the energy landscape thereby eliminating high energetic configurations and focusing on the lowest energy configurations as the starting/final point for the dissociation process. The most stable adsorption/co-adsorption configurations for H_2S and HS + H/2H + S respectively are employed as initial and final states. Based on our earlier analysis of adsorption energetics leading to fragmented configurations, we explored a number of pathways leading to these dissociation states. Our investigation proceeded with the most physical dissociation pathways. We present two pathways to the dissociation of H_2S into HS + H on Fe(110) surface. The reaction energy profile for the dissociation process through the different pathways are shown in Fig. 4. The first possible pathway (referred to as Path 1 hereafter) for the dissociation of H_2S into HS/H (Eq. (2)) initiates the process from the R45@LB (Fig. 2(e)), after the incident H_2S molecule is absorbed with an adsorption energy of −0.6 eV. The adsorption is followed by tilting of the H_2S molecule away from the LB site. At the transition state (TS1), the H-S bond for the dissociated H atom increased from 1.38 to 1.91 Å while that for the undissociated H atom merely increased by 0.01 Å. After TS1 the dissociated H atom moves to the adjacent LB site leaving the HS moiety at the initial LB site, requiring a barrier of 0.16 eV. An alternative route (referred to as Path 2 hereafter) initiates the dissociation from the next most stable adsorption site, R00@SB. A higher barrier of 0.2 eV (TS2) is needed for the dissociation of H_2S into HS/H. Apart from identifying the lowest energy configurations for the initial and final states leading to the dissociation, it is also important to take into account small changes in the orientation of the H_2S molecule and how it affects the energy landscape since this may have significant effect on the reaction energetics. For instance the diffusion of H_2S from R45@LB to R00@SB (see Figure S1 in the supporting material) can affect how the molecule dissociate consequently affecting the energetics and reaction kinetic. We found a diffusion barrier of 0.14 eV for the diffusion of H_2S from R45@LB to R00@SB. Dissociation via this channel (referred to as Path 3 hereafter) will include the diffusion of the H_2S molecule to the R45@LB first, see Fig. 6.

In the next stage (Eq. (3), dissociation of HS into H/S), the process commences from the most favorable adsorption configuration for HS: the HS moiety occupying the LB site and H at TF. The process proceeds with the severance of the H-S bond and consequently the S and H are adsorbed on the surface individually. The most stable arrangement for the final configuration involves the H adsorbed at the TF and the S adsorbed at the LB. This configuration is reached by overcoming a barrier of 0.12 eV. At the transition state for this reaction the H-S bond is broken and consequently new Fe-H and Fe-S bonds are formed. The newly dissociated H atom is at a distance 2.1 Å from the S atom, a 32% increase in the bond length compared to the free state of HS (see Fig. 5).

Analysis of the dissociation barrier of H_2S and the adsorption energetics shows that the dissociation is facile on the Fe (110) surface. Evidently, depending on the initial configuration at the initiation of the dissociation process different conclusions can be obtained thereby underlying the influence of the orientation of molecule in evaluating minimum energy path of reactions like this.

Comparison of our adsorption energies, dissociation energy and elementary processes involved in the dissociation of H_2S with previous work [31] on Fe(100) confirms that the reactivity of H_2S on Fe surface is dependent on the surface morphology. Notably, our calculated dissociation barrier for H_2S on Fe (110) is lower than the values reported for Fe(100) [30]. Similar trend has been established for different metal

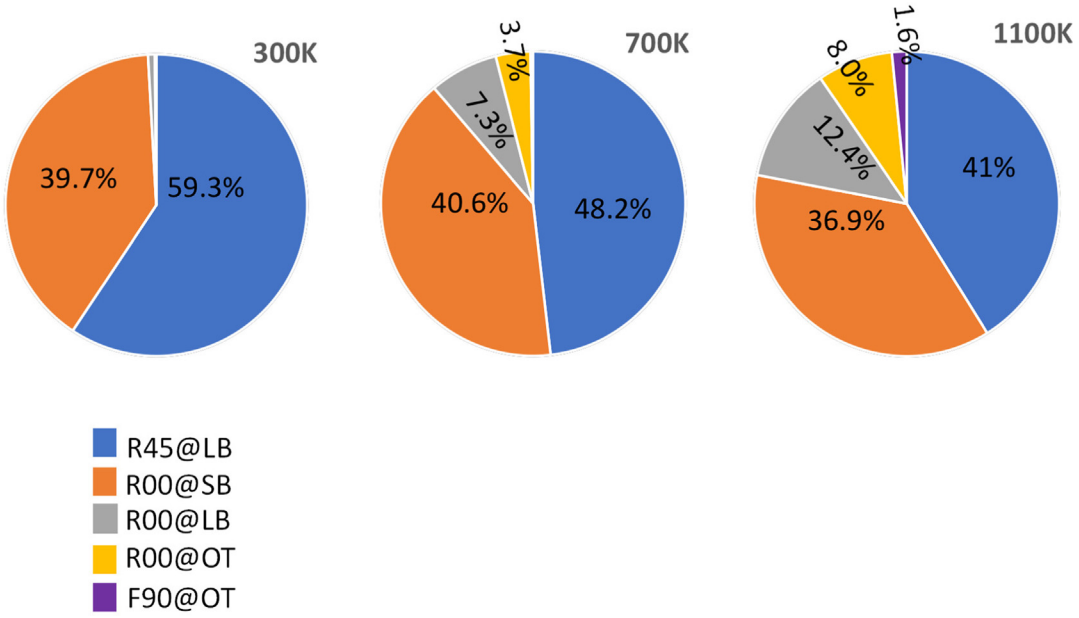

Fig. 4. Pie chart showing probability of molecule sticking for each of the configurations shown in Fig. 2.

surfaces [43,44] and is related to the coordination number of the surface metal atoms. Interestingly, none of the previous work investigated the effect of co-adsorbed H on the energetics discussed.

3.4. Reaction kinetics

Having explored extensively the different adsorption scenarios and the competition between the representative adsorption, we investigate the rate determining step to the complete dissociation, aimed at understanding the limiting elementary step to the blocking effect. The calculated rate is shown in Table 3.

The variation in temperature has been reported to alter the dissociation mechanism, determined species formed and surface reactions that occur, hence temperature as high as 1080 K has been considered in the simulation of the H_2S dissociation on Fe surface [15,45,46].

Table 3
Dissociative rate constant (s^{-1}) for the adsorption H_2S at different temperature in K.

Reaction	Path	300 K	700 K	1100 K
$H_2S \rightarrow HS + H$	Path 1	1.7×10^{-3}	6.4×10^{-2}	1.7×10^{-1}
	Path 2	3.4×10^{-4}	3.2×10^{-2}	1.1×10^{-1}
	Path 3	1.2×10^{-6}	2.9×10^{-3}	2.4×10^{-2}
$HS + H \rightarrow H + S + H$		8.2×10^{-3}	1.3×10^{-1}	2.7×10^{-1}

Our calculated rate for reaction 2 (paths 1, 2, 3) reveal a lower dissociative rate for path 3 followed by path 2 and path 1 having the highest rate. Despite the very low difference in energy barrier between paths 1 and 2 (0.04 eV) the dissociative reaction rate constant is 5, 2, 1.5 times larger for path 1 at 300 K, 700 K and 1100 K respectively, see

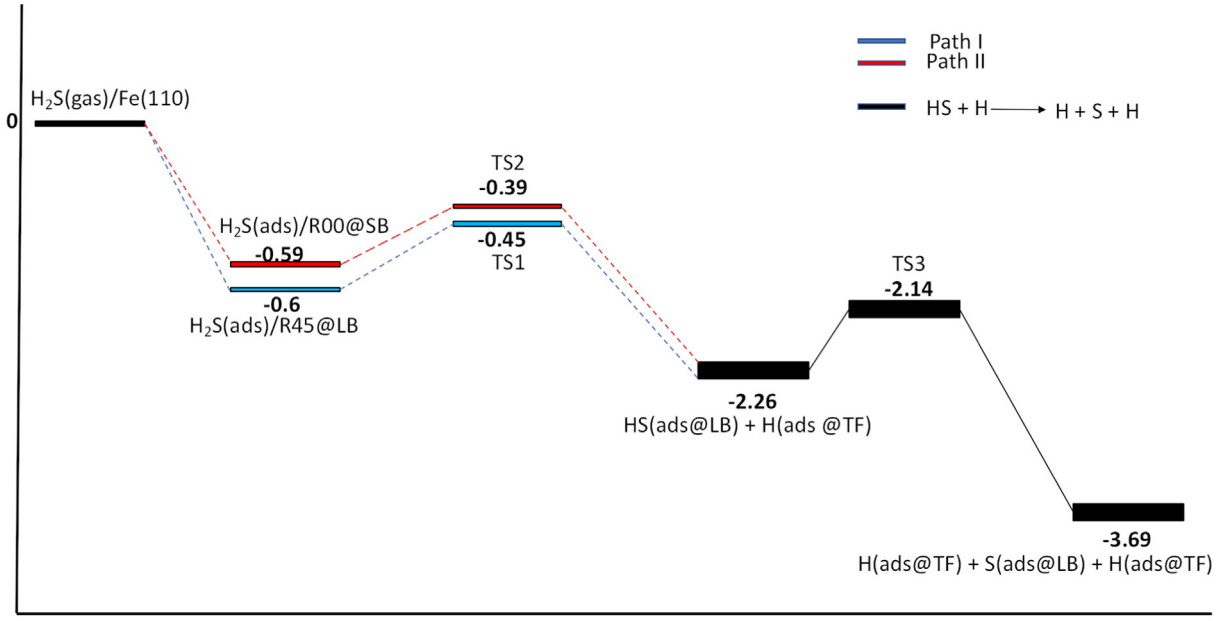

Fig. 5. Reaction energy diagram for H_2S dissociation on Fe(110) for paths 1 and 2 showing the elementary reaction sites through each of the 2 paths. The images R45@LB, R45@LB are shown in Fig. 2c and d respectively while the configuration for HS + H and H/S/H are shown in Fig. 3b and 3c respectively.

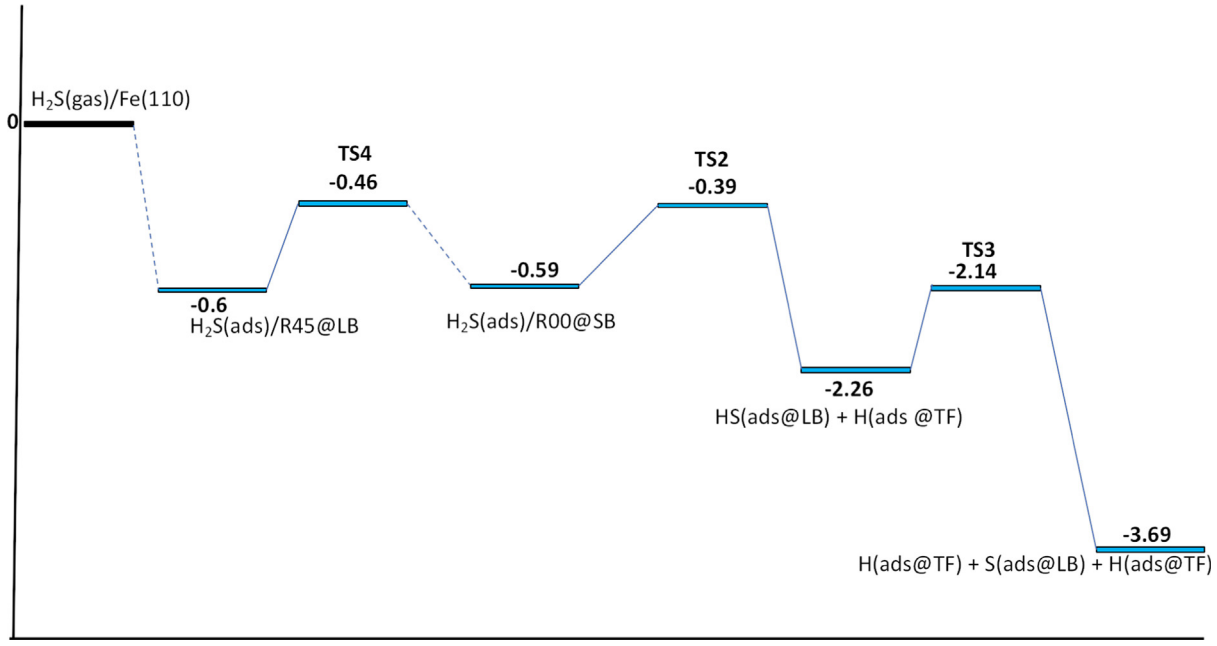

Fig. 6. Reaction energy diagram for H_2S dissociation on Fe(110) for path 3 showing the diffusion barrier for R45@LB to R00@SB leading to the complete dissociation process. The images R45@LB, R45@LB are shown in Fig. 2c and d respectively while the configuration for HS + H and H/S/H are shown in Fig. 3b and c respectively.

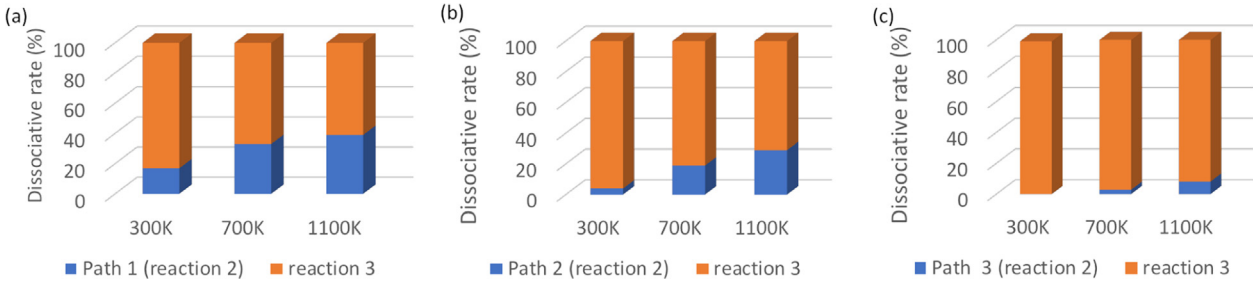

Fig. 7. Temperature dependence of the dissociative rate initiated from the three pathways leading to the complete decomposition.

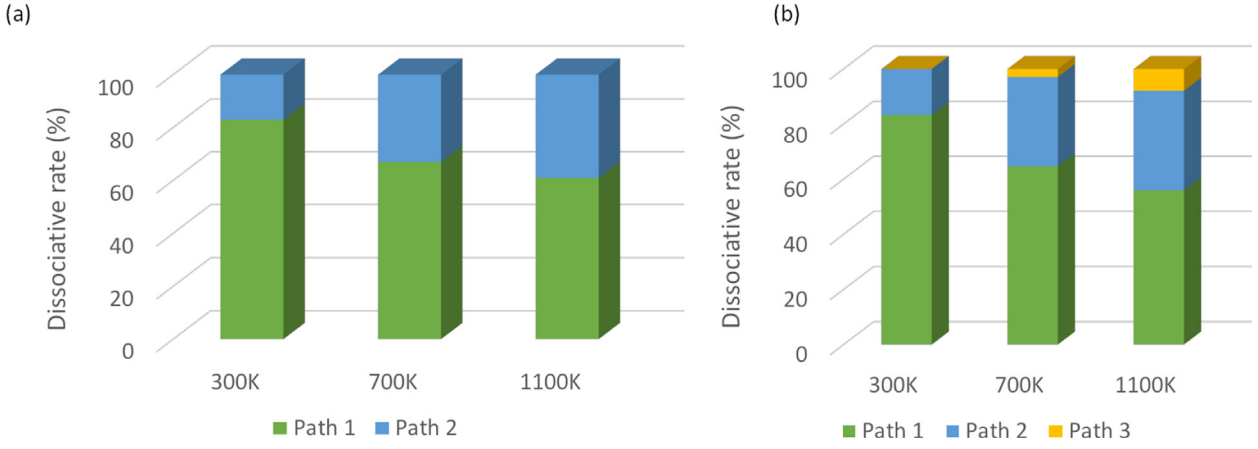

Fig. 8. Temperature dependence of the competition in dissociative rate (reaction 2) between process initiated from path 1 and path 2 (a) and involving path 3 (b).

Table 3. It therefore follows that in this reaction the lower the barrier, the higher the dissociative rate constant and vice versa. A comparison of the dissociative rate for the complete dissociative reaction as a function of the paths followed for reaction 2 is shown in Fig. 6. The rates are always higher for reaction 3 (low barrier) irrespective of the path followed for reaction 2 to occur. Clearly, reaction 3 occurs at a much faster rate than reaction 2 thereby making reaction 2 the rate determining step for the complete dissociation of H_2S on Fe (110) surface. Worthy of note however, is the reduction in the dissociative rate for reaction 3 moving from path 3 to path 1 at 1100 K. There is an obvious competition emerging between path 1 and path 2 as temperature is raised. Fig. 7(a) shows the competition between the dissociative rates for paths 1 and 2 assuming the processes occur simultaneously. The rates are lower for path 2 with dissociation via path

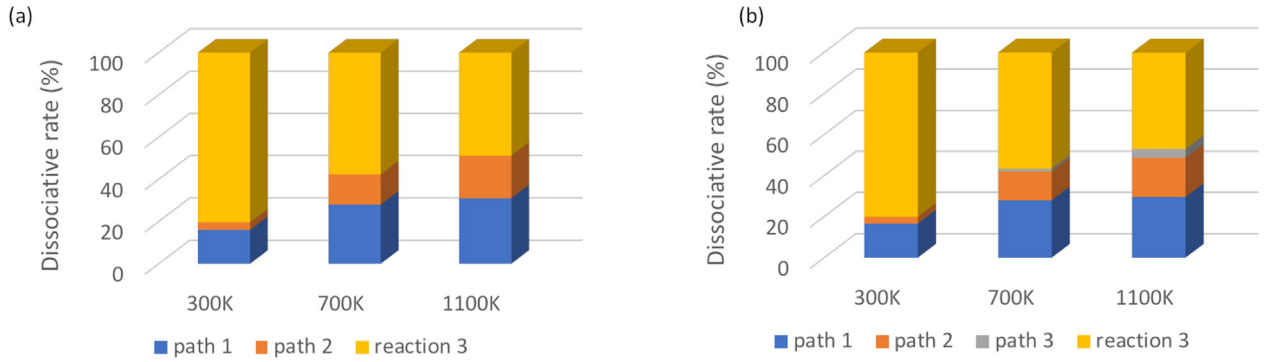

Fig. 9. Temperature dependence of the competition in dissociative rate for complete dissociation. Process initiated from path 1 and path 2 only are shown in (a) and including path 3 shown in (b).

1 dominating. Analysis including path 3 (See Fig. 7(b)) only affect the trend minimally with path 1 still occuring at a faster rate. Similar analysis for the complete dissociative rate and competition is shown in Fig. 8(a and b). It confirmed our earlier finding that the reaction 3 occurs at a faster rate and that including path 3 only affects the dissociative rate slowly. Therefore, the choice of the starting position for the dissociation ultimately determines if a reaction is spontaneous or not and has serious implications on the final conclusion reached with regards to the calculation of minimum energy pathways for dissociation of H_2S (see Fig. 9).

We have shown how the orientation of H_2S affects the adsorption, dissociative energetics, and ultimately the conclusion reached in Fe (110) surface. This approach will open door for accurate atomistic simulation of molecules on surfaces. As discussed earlier, results obtained here are in general agreement with experiments and DFT calculations when similar starting configurations are employed. Using larger simulation cells, to decrease finite-size effects, and offering an extensive characterization of the energy landscape does not also qualitatively affect the trends discussed in this work. The small dissociation barrier obtained for H_2S shows that it is an aggressive attacker of iron. Previous works [30,31,25] on dissociation of H_2S on Fe(110) have reported different barriers. The starting position for the dissociation in the mentioned previous work is different thereby highlighting the importance of an holistic consideration of all possible orientations of the molecule in calculations like this. Interestingly, our calculated barrier is still lower than that previously reported for Fe(100), which is a more open structure. Similar observation was reported for the dissociation of water on Pt [47] and Ni[48] surfaces. They showed that the barrier for dissociation of H_2O is lower in 110 facet than in the more open 100 facet. There have been reports on experimental studies of H_2S adsorption on Fe surfaces [15,49,50]. Specifically, X-ray photoelectron spectroscopy (XPS) [15] studies of H_2S on Fe(110) showed that H_2S adsorption is molecular at 110 K but dissociative from 190 K up to ambient temperatures. This observation is also supported by the work of Kalador et al. [49] where, using low energy electron diffraction (LEED) they observed dissociative adsorption of H_2S at 150 K. Young et al. [50] studied the sulfidation of Fe films and found that the reaction is solid-state diffusion controlled (by Fe ions) with the bulk diffusion barrier higher than the H_2S dissociation barrier. All these indicates the ease of dissociation of H_2S on Fe. Our calculated adsorption energy and dissociation barrier shows that H_2S is weakly adsorbed on Fe (110) and would preferentially dissociate on Fe(110) surface. Grabke et al. [1] also found that a small concentration of H_2S is sufficient to slowdown the metal dusting process. This could be unrelated to the facile deposition of S atoms that block the surface sites for CO adsorption and/or dissociation. Our result is consistent with this idea. Hence, while carbon monoxide has been identified as the main culprit for high-temperature corrosion phenomena like metal dusting, a comparison of our calculated energetics and those from CO on Fe surface shows that H_2S reacts faster than CO and hence could be a viable source of S for blocking reaction sites where CO reactions would take place.

4. Conclusion

Motivated by the finding that the adsorption of S on Fe surface helps to block reaction sites causing its carburization, an atomic scale study on the dissociation of H_2S molecule on Fe (110) have been conducted. Our finding shows that H_2S is dissociated via the successive severance of the H-S bond thereby producing the surface S absorbed at the LB. The adsorption of H_2S was found to be exothermic with the computed energetics found to be strongly dependent on the starting orientation of the H_2S molecule with some cases of the adsorption found energetically degenerate. The role of the molecular orientation is confirmed and found to be crucial to the mode of adsorption; as a molecule or as fragmented moieties. We also find the rate determining step to this reaction to be the first deprotonation process, although depending on the path where the reaction is initiated from there are competitions in the rate of dissociation as temperature is raised. The information obtained about the complete decomposition process are difficult to obtain from experiment hence indicating the vital role of ab initio studies in the design of improved materials for the inhibition of metal dusting on metal surface.

Declaration of Competing Interest

The authors declare that they have no known competing financial interests or personal relationships that could have appeared to influence the work reported in this paper.

Acknowledgement

The advanced computing facility of Texas A & M University at Qatar is used for all calculations. This work is supported by the Qatar National Research Fund (QNRF) through the National Priorities Research Program (NPRP) under project number NPRP10-0105–170118. Authors are thankful to fruitful discussions with Nick Laycock, Abitha Ramesh and Normand Mousseau.

Appendix A. Supplementary material

Supplementary data associated with this article can be found, in the online version, at https://doi.org/10.1016/j.apsusc.2020.147470.

References

[1] H. Grabke, C. Bracho-Troconis, E. Müller-Lorenz, Mater. Corros. 45 (1994) 215–221.
[2] D.J. Young, J. Zhang, JOM 64 (2012) 1461–1469.
[3] H.J. Grabke, E.M. Müller-Lorenz, A. Schneider, ISIJ Int. 41 (2001) S1–S8.

[4] others,, et al. Metal Dusting-Severe Problem in Operation of Syngas Generation for GTL Plant, in: The Fifteenth International Offshore and Polar Engineering Conference, 2005.
[5] I.H. Sahputra, A. Chakrabarty, O. Restrepo, O. Bouhali, N. Mousseau, C.S. Becquart, F. El-Mellouhi, Phys. Status Solidi (b) 254 (2017) 1600408.
[6] X. Chen, N. Birbilis, T. Abbott, Corrosion 67 (2011) 035005–1.
[7] A. Schneider, H. Grabke, Mater. Corros. 54 (2003) 793–798.
[8] H. Grabke, D. Moszynski, E. Müller-Lorenz, A. Schneider, Surf. Interface Anal.: An Int. J. Devoted Develop. Appl. Tech. Anal. Surf., Interfaces Thin Films 34 (2002) 369–374.
[9] T.A. Ramanarayanan, C. Chun, ECS Trans. 41 (2012) 47–60.
[10] G. Hultquist, B. Tveten, E. Hörnlund, M. Limbäck, R. Haugsrud, Oxid. Metals 56 (2001) 313–346.
[11] A. Agüero, M. Gutiérrez, L. Korcakova, T. Nguyen, B. Hinnemann, S. Saadi, Oxid. Metals 76 (2011) 23–42.
[12] K. Yoshihara, Hyomen Kagaku 6 (1986) 388–399.
[13] H. Grabke, EUROCORR'97, 1997, 2, 1–8.
[14] D. Jiang, E.A. Carter, Surf. Sci. 583 (2005) 60–68.
[15] P. Narayan, J. Anderegg, C. Chen, J. Electron. Spectrosc. Relat. Phenom. 27 (1982) 233–242.
[16] D.S. Lauretta, K. Lodders, B. Fegley Jr., D.T. Kremser, Earth Planet. Sci. Lett. 151 (1997) 289–301.
[17] Z. Zhi, Q. Luo, Z.L. Ran, T.H. Shi, First principles calculation on adsorption of S on Fe (100), Adv. Mater. Res. (2011) 690–694.
[18] H. Shih, F. Jona, D. Jepsen, P. Marcus, Phys. Rev. Lett. 46 (1981) 731.
[19] I.M. Bernstein, A.W. Thompson, Warrendale, PA, Metall. Soc. AIME, 1981, 1071 p 1981.
[20] D.R. Alfonso, A.V. Cugini, D.C. Sorescu, Catal. Today 99 (2005) 315–322.
[21] M.J. Spencer, I.K. Snook, I. Yarovsky, J. Phys. Chem. B 110 (2006) 956–962.
[22] X. Zhou, B. Kolb, X. Luo, H. Guo, B. Jiang, J. Phys. Chem. C 121 (2017) 5594–5602.
[23] D.R. Alfonso, Surf. Sci. 602 (2008) 2758–2768.
[24] A. Chakrabarty, O. Bouhali, N. Mousseau, C.S. Becquart, F. El-Mellouhi, J. Appl. Phys. 120 (2016) 055301.
[25] L. Ren, Y. Cheng, R. Shao, X. Meng, J. Yang, Q. Wang, Appl. Surf. Sci. 500 (2020) 144232.
[26] G. Kammlott, J. Franey, T. Graedel, J. Electrochem. Soc. 131 (1984) 505.
[27] S. Chen, S. Sun, B. Lian, Y. Ma, Y. Yan, S. Hu, Surf. Sci. 620 (2014) 51–58.
[28] Q.-L. Tang, S.-R. Zhang, Y.-P. Liang, J. Phys. Chem. C 116 (2012) 20321–20331.
[29] X. He, Y. Gui, J. Xie, X. Liu, Q. Wang, C. Tang, Appl. Surf. Sci. 500 (2020) 144030.
[30] D. Jiang, E.A. Carter, J. Phys. Chem. B 108 (2004) 19140–19145.
[31] X. Wen, P. Bai, Z. Han, S. Zheng, B. Luo, T. Fang, W. Song, Appl. Surf. Sci. 465 (2019) 833–845.
[32] G. Kresse, J. Furthmüller, Phys. Rev. B 54 (1996) 169.
[33] M. Ernzerhof, G.E. Scuseria, J. Chem. Phys. 110 (1999) 5029–5036.
[34] S. Liu, X. Tian, T. Wang, X. Wen, Y.-W. Li, J. Wang, H. Jiao, PCCP 17 (2015) 8811–8821.
[35] T. Ossowski, J.L. Da Silva, A. Kiejna, Surf. Sci. 668 (2018) 144–149.
[36] J. Moellmann, S. Grimme, J. Phys. Chem. C 118 (2014) 7615–7621.
[37] S.P. Ong, W.D. Richards, A. Jain, G. Hautier, M. Kocher, S. Cholia, D. Gunter, V.L. Chevrier, K.A. Persson, G. Ceder, Comput. Mater. Sci. 68 (2013) 314–319.
[38] H. Jónsson, G. Mills, K.W. Jacobsen, 1998.
[39] G. Henkelman, B.P. Uberuaga, H. Jónsson, J. Chem. Phys. 113 (2000) 9901–9904.
[40] J.L. Fajín, M.N.D. Cordeiro, F. Illas, J.R. Gomes, J. Catal. 268 (2009) 131–141.
[41] R.J. Broos, B. Klumpers, B. Zijlstra, I.A. Filot, E.J. Hensen, Catal. Today 342 (2020) 152–160.
[42] T. Usman, M.-Q. Tan, Adsorption 24 (2018) 563–574.
[43] F. Delbecq, P. Sautet, Surf. Sci. 295 (1993) 353–373.
[44] X.-Y. Pang, C. Wang, Y.-H. Zhou, J.-M. Zhao, G.-C. Wang, J. Mol. Struct. (Thoechem) 948 (2010) 1–10.
[45] E.T. Bentria, G.K. N'tsouaglo, C.S. Becquart, O. Bouhali, N. Mousseau, F. El-Mellouhi, Acta Mater. 135 (2017) 340–347.
[46] C.M. Chun, J. Mumford, T. Ramanarayanan, J. Electrochem. Soc. 149 (2002) B348.
[47] J.L. Fajín, M.N. DS Cordeiro, J.R. Gomes, J. Phys. Chem. A 118 (2014) 5832–5840.
[48] J.L. Fajín, M.N.D. Cordeiro, F. Illas, J.R. Gomes, J. Catal. 276 (2010) 92–100.
[49] S. Kelemen, A. Kaldor, J. Chem. Phys. 75 (1981) 1530–1537.
[50] D. Young, W. Smeltzer, J. Electrochem. Soc. 123 (1976) 229.